†Electronic supplementary information for

Thermally Robust and Optically Transparent Infrared Selective Emitter for Compatible Camouflage

Lei Zhang, Jun Wang, Jing Lou, Ying Zhu, Boheng Gui, Mingde Feng, Jiafu Wang, and Shaobo Qu**

Department of Basic Sciences, Air Force Engineering University, Xi'an 710051, P. R. China.

E-mail: wangjun563@163.com; qushaobo@mail.xjtu.edu.cn

Note S1. Samples fabrication and additional characterization

ITO and ZnS films were deposited on 100 mm × 100 mm glass substrates by magnetron sputtering (Kurt. J. Lesker). In this procedure, DC sputtering for ITO film and RF sputtering for ZnS film was implemented, respectively. The used sputtering targets are 76.2 mm diameter zinc sulfide (99.99%) and indium tin oxide (90wt.%In_2O_3~10wt.%SnO_2, 99.99%) produced by Laiyan technology Hebei Co., Ltd (Hebei, China). Before opening the shelter, the sputtering targets require 10 minutes of pre-sputtering to remove surface contaminants. During deposition process, injecting 20 sccm of pure Ar into the chamber as a working gas flow, and the working pressure is maintained at 6 mTorr. The RF sputtering power is set to 115W (2.5W/cm^2), in which the refractive index and visible transmittance of the films are stable. For DC sputtering, the oxygen-argon-ratio (O_2:Ar) was set to 1:40 to favor ITO film growth. To assure the uniformity of the deposited films, the rotational speed of the disk for sputtering is set to 20 rpm and the substrate temperature is set to 573 K. This temperature is sufficient for stable crystallization of the two materials. Then, the films were cooled naturally in the vacuum chamber without additional annealing process.

These phase structures were detected by X-ray diffraction (XRD, XRD-7000, Shimadzu). As shown in **Figure S1a**, the XRD patterns indicates that only these two classes of components are contained. For the preparation of single ZnS film, as the substrate temperature increased from room temperature to 473 K, the film crystallinity was improved due to the increase in thermal stress and surface diffusivity of sputtered particles.[1] The crystallinity is beneficial for enhancing the thermal stability of the composite films. There is a slight decrease in the peak intensity for (111) orientation of single ZnS film compared with samples #1 and #2. Causing the change of particle kinetic energy with temperature may be the difference of film

crystallinity.[1,2] The difference between the corresponding peak intensities of samples #1 and #2 derives from the different thickness of the top ZnS. These composite multilayer-film structures were prepared without additional annealing procedures, further demonstrating that these two materials can be steadily crystallized and reducing the complexity of fabrication procedure.

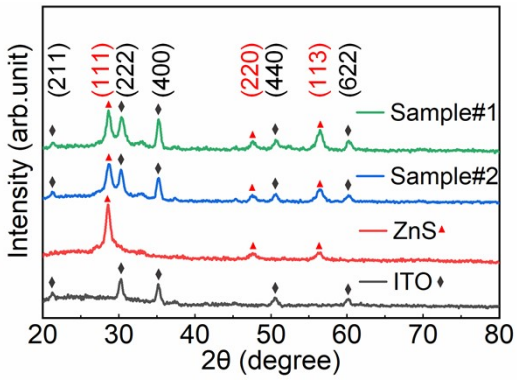

Figure S1. Film characterization. (a) The XRD patters of single films and composite films.

For the application of general low-emissivity materials, the two critical factors, conductivity and surface roughness, were analyzed by optical theory. In optical theory, the relationship between reflectivity and conductivity of the single film is as follows:[3]

$$\tau = \left(1 - \frac{2}{n+1}\right)^2 \tag{1}$$

$$n^2 = \frac{\mu}{2}\left\{\left(\sqrt{\varepsilon^2 + \frac{4\sigma^2}{v^2}}\right) + \varepsilon\right\} \tag{2}$$

where τ and σ means the reflectivity and conductivity, respectively. n is the refraction index, ε is the permittivity, μ is the permeability, and v is the Planck's constant. Under thermal equilibrium conditions, the absorption and emissivity of the object is equal. Since the transmission is zero in this design, the emissivity/absorption spectra are calculated by the following formula[4]: $\varepsilon(\lambda,T)=\alpha(\lambda,T)=1-\tau(\lambda,T)$ where $\varepsilon(\lambda,T)$, $\alpha(\lambda,T)$, and $\tau(\lambda,T)$ stand for the emissivity, absorption, and reflectivity, respectively.

As shown in **Figure S1b and S1c**, the images of atomic force microscopic (AFM, MFP-30

Classic, OXFORD) scan of the ITO (sample #2, ITO/ZnS/ITO) and ZnS (sample #1, ITO/ZnS/ITO/ZnS) surface showing rms roughness are about ±20 nm and ±30 nm, respectively. The relationship between reflectivity and roughness can theoretically be described as:

$$R_r = R_P exp\left[-\left(\frac{4\pi\sigma}{\lambda}\right)^2 \right] \tag{3}$$

where R_r and R_P are the reflectivity for a rough and polished surface, respectively. σ is surface roughness and λ is wavelength. In 2.5~14μm, the rms roughness is acceptable in service. Generally, increasing conductivity and reducing roughness can effectively minimize the emissivity of conductive films.

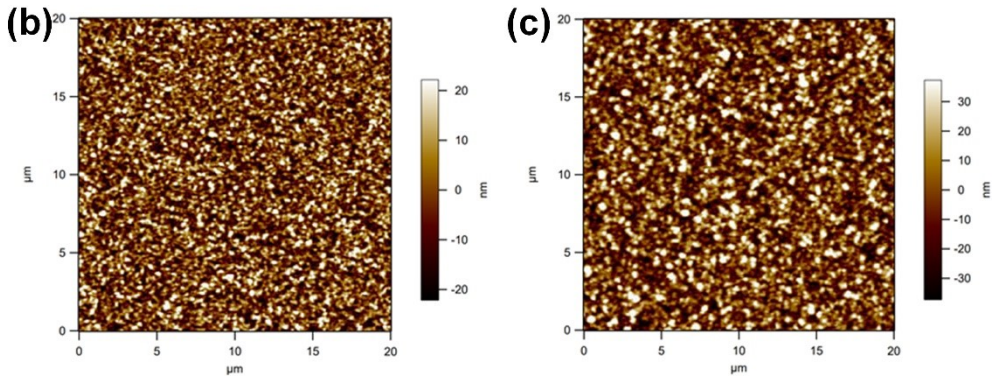

Figure S1. Film characterization. The atomic force microscopy images of Sample #2 (b) and sample #1 (c).

Note S2. Analysis of design principle

In this work, transparent conductive film of indium tin oxide (ITO) and dielectric film of zinc sulfide (ZnS) are adopted to composite four-layer structure for camouflage in infrared and visible regions. ITO, as a transparent conductive film, is widely used in the field of electronics and photonics, and all the applications are around its excellent visible transmittance and conductivity. The two factors, photonic band gap and plasma oscillation frequency, determine the spectral absorption and reflection, respectively. ZnS, as an excellent infrared transmissive dielectric, is widely used in the field of military, such as the infrared window of a detector,

infrared imaging system, and infrared lidar sealing cover, etc. Herein, the Drude model was employed to describe the plasma characteristics of ITO shown in **Figure S2a**. ITO possesses negative permittivity in 2.5~14 μm, further indicating that ITO thin film is similar to metal film in IR band.[4] Due to the size effect of ITO film, ITO with a thickness of 100 nm possesses semi-transmissive property in mid-wave infrared (2.5~5 μm), which allow partial penetration of IR beams like a frequency selective surface. ITO with a thickness of 300 nm possesses almost zero transmission, as shown in **Figure S2b**. Thus, ITO film with a thickness of 300 nm can be used as a reflective layer (square resistance of about 5 $\Omega \cdot sq^{-1}$), and ITO film with a thickness around 100 nm (square resistance of about 15 $\Omega \cdot sq^{-1}$) is employed as lossy layer.[5] The size effect of ITO film was adopted to generate an ITO/dielectric/ITO resonant cavity, which can yield resonant peaks that the resonant wavelength is determined by refraction index *n* and thickness of the dielectric spacer.

In mid-infrared range (2.5~25 μm), there are two non-atmospheric windows in 2.5~3 μm and 5~8 μm. In these two windows, IR radiation of an object can be readily absorbed by polar molecules (H_2O and CO_2) in the atmosphere. The dual non-atmospheric windows absorption can be achieved by designing resonant peaks in 2.5~3 μm and 5~6 μm through ITO/dielectric/ITO resonator. As shown in **Figure S2c**, the two resonant peaks of the proposed design satisfy the relationship of frequency doubling. The intensity of the two absorption peaks would be enhanced when the thickness of the lossy ITO layer is decreasing. However, enhanced absorptions will lead to the increase of emissivity in 8~14 μm, as demonstrated in **Figure S2d**. Therefore, the thickness of t3 was chosen in the range of 100 to 120 nm to ensure low emissivity of this emitter in the detectable band. As discussed above, the thickness of reflective ITO and lossy ITO were selected as 300 nm and 100 nm, respectively.

To find the optimal values of the structure, the simulated spectra of the ITO/ZnS composite samples in wavelength of 2.5~14 μm were investigated by commercial electromagnetism simulation software CST. The thicknesses of top ZnS and ZnS spacer were optimized using the genetic algorithm built into CST. With the step size set to 10 nm, it can be found that the four alternating layers of ITO/ZnS/ITO/ZnS with thickness of 300/1000/100/550 nm possesses remarkable selective emissivity.

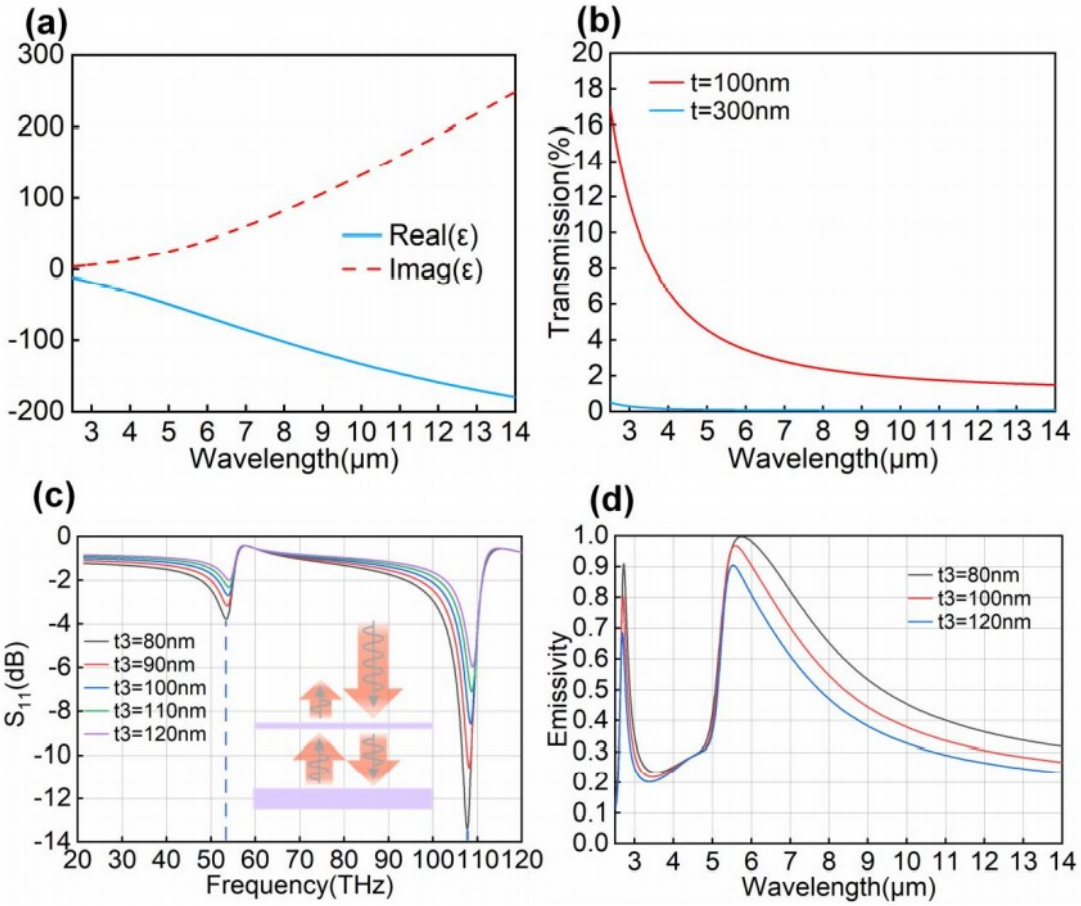

Figure S2. Analysis of design principle. (a) The equivalent permittivity of ITO in 2.5~14 μm. (b) The transmission of ITO film with different thickness. (c) Reflection coefficient S11 of ITO/dielectric/ITO resonator with different thickness of lossy ITO. (d) The simulated spectra of designed emitter with different t_3.

Note S3. The spectra of Structures with different layers

ITO with a thickness of 300 nm was selected as the reflective backplane. When ITO is covered with a layer of infrared transmissive dielectric film (ZnS), the reflectance can be

improved at specific frequency due to half-wave loss, as shown in **Figure S3a**. At around 5 μm, the enhanced reflectance of two-layer structure is higher than single ITO film, where the thickness of dielectric film is 1 μm. The 1 μm corresponds to the minimum thickness ($t_4 = \frac{k\lambda}{2n}$, $k = 1$) of the reflective film at around 2.5 μm (peak 1) and 5 μm (peak 2), further proved that the mechanism of reflective film is suitable for explaining the two-layer structure. Moreover, reflective film can be adopted to design lower emissivity at specific frequency. As an ISE, the two-layer structure of ITO/ZnS cannot exhibit ramarkable selective emissivity for infrared camouflage. The spectral emissivities corresponding to the four structures are shown in **Figure S3b**, which clearly shows the necessity and superiority of ITO/ZnS/ITO/ZnS four-layer composite films.

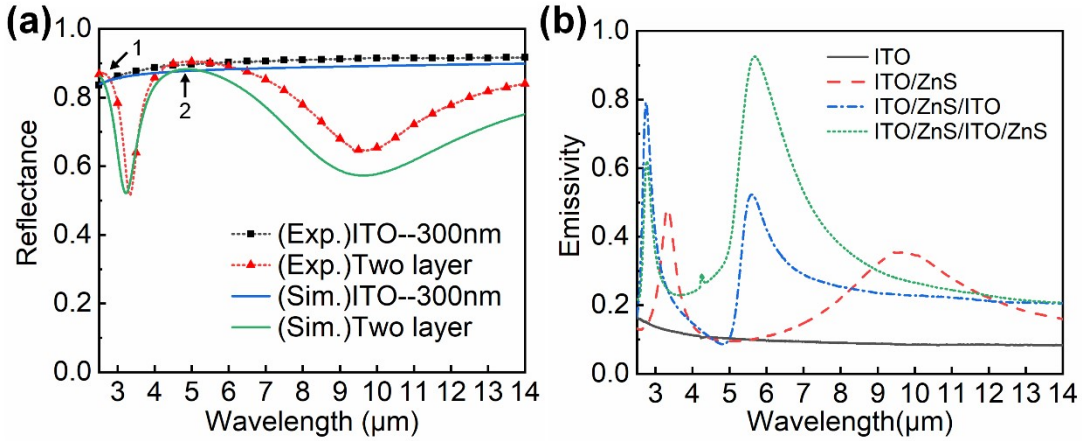

Figure S3. The reflectance spectra and emissivity spectra of different structures. (a) The spectral reflectance of single ITO film with thickness of 300 nm and two-layer structure of ITO/ZnS (300/1000 nm). (b) The spectral emissivity with different structure of ITO, ITO/ZnS, ITO/ZnS/ITO, and ITO/ZnS/ITO/ZnS (300 nm, 1000 nm, 100 nm, 550 nm, respectively).

Note S4. Atmospheric transmission simulated by MODTRAN

In this work, simulation software of MODTRAN was employed to analyze atmospheric transmission spectra, which using general models for atmospheric transmission with an accuracy of 2 cm^{-1}. As shown from **Figure S4a** to **S4d**, the spectral atmospheric transmission

possesses obvious wavelength selective properties in infrared band with different parameters. The reduction of spectral transmission in 2.5~3 μm and 5~8 μm mainly result from the absorption of polar molecules (H_2O and CO_2, etc.) and the scattering of aerosols. By applying different observed height, atmospheric model, and aerosol model, it is demonstrated that these selective properties of atmospheric transmission spectra are universal. As comparison, the spectral atmospheric transmission does not exhibit selective properties in visible band, which explains that the atmosphere is transparent rather than colored. As shown in **Figures S4e** and **S4f**, it can be found that the effect of observed height is more significant than that of season (temperature) and aerosols.

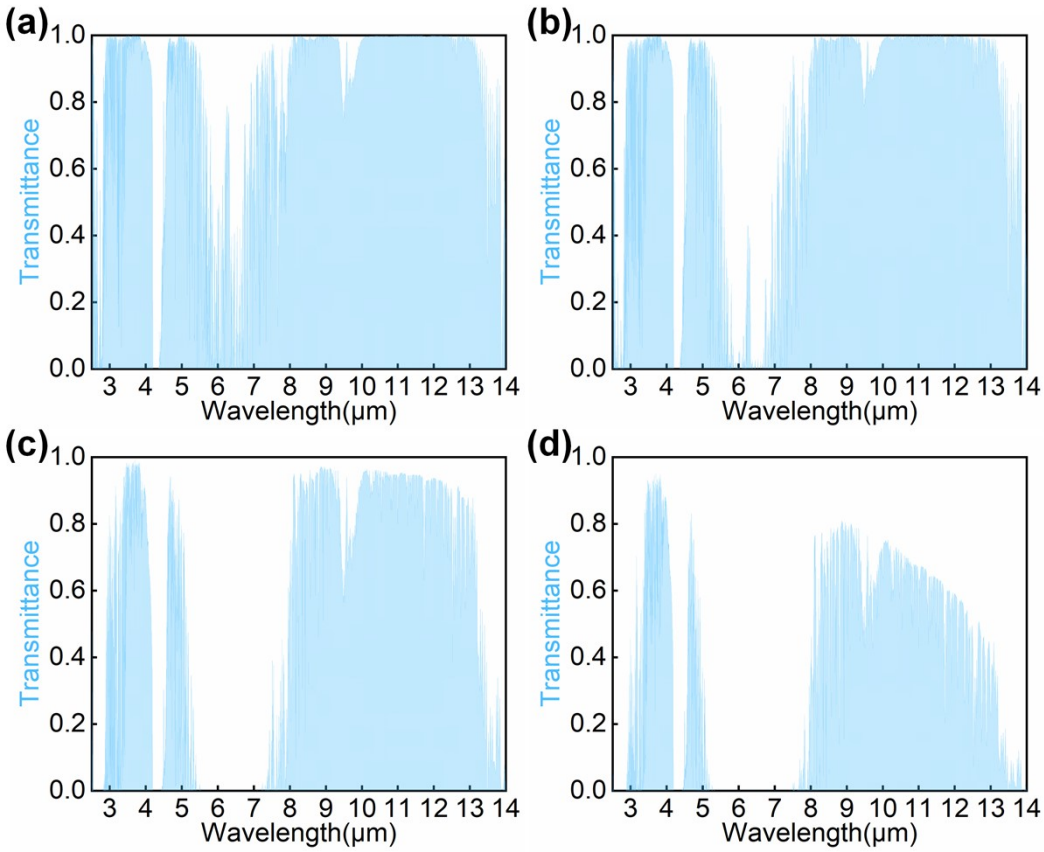

Figure S4. The atmospheric transmission spectra with different parameters in 2.5~14 μm infrared band. (a) High obversed positon, middle latitude winter atmospheric model, and no aerosol or clouds. (b) High obversed position, middle latitude summer atmospheric model, and rural aerosol model. (c) Low obversed position, middle latitude winter atmospheric model, and no aerosol or clouds. (d) Low obversed position, middle latitude summer atmospheric model, and rural aerosol model.

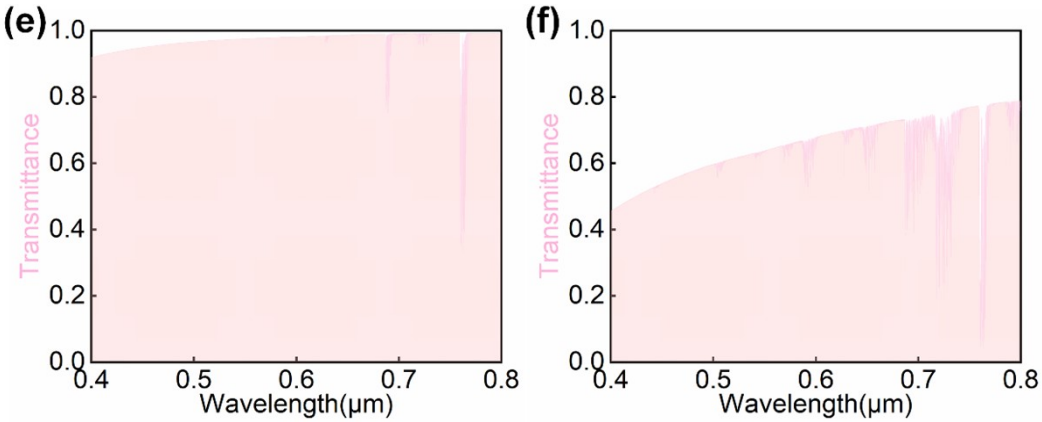

Figure S4. The atmospheric transmission spectra with different parameters in 0.4~0.8 μm visible band. (e) High obversed positon, middle latitude winter atmospheric model, and no aerosol or clouds. (f) Low obversed position, middle latitude summer atmospheric model, and rural aerosol model.

Note S5. The measured spectra of all samples

In this work, four groups of samples with t_4 thickness of 550 nm, 0 nm, 50 nm and 750 nm were prepared for measurement. They were numbered as sample #1, sample #2, sample #3 and sample #4, respectively. As **Figure S5a** shown, we selected three test areas in each sample for measurement of emissivity at room temperature, and the emissivity spectrum were averaged from the three spectra (The diameter of areas A, B and C is 3 cm). The measured spectra of the four groups of samples are shown in **Figure S5b**. Compared with the other samples, sample #1 exhibits better wavelength selective property apparently, indicating that the top dielectric layer (ZnS) is beneficial for modulating selective emission. Especially, the average emissivity of sample #4 is greater than that of sample #1, which means that we can visually observe the modulation effect of t4 on the emissivity through the infrared camera working in 8~14 μm.

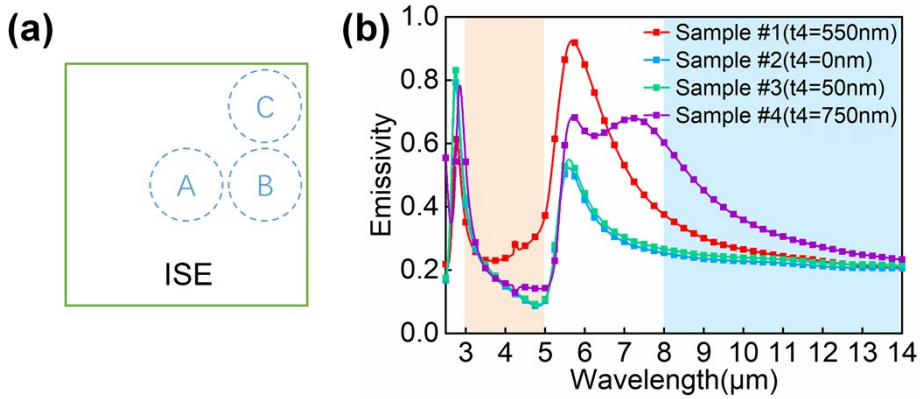

Figure S5. (a) The sampling areas of fabricated ISE. (b) The measured emissivity spectra of the four groups of prepared samples.

Note S6. Evaluation of camouflage performance

We evaluated the camouflage performance (CP) of the ITO/ZnS/ITO/ZnS composite film based selective emitter from the perspective of radiative energy and revealed the robustness.[6] According to Planck radiation law, the spectral emissive power of blackbody can be calculated as follows:[7]

$$E_{b\lambda}(\lambda,T)=\frac{2\pi hc_0^{\ 2}}{\lambda^5\left[exp\left[\frac{hc_0/k}{\lambda T}\right]-1\right]} \tag{4}$$

where the $E_{b\lambda}$, $2\pi hc_0^{\ 2}$, hc_0/k, λ, and T stand for the spectral blackbody emissive power, the first radiation constant (C1=3.7418×108W·μm4·m-2), the second radiation constant (C2=14388μm·K), wavelength and temperature, respectively. For a object, the emissive power through λ1~λ2 can be calculated by formula:

$$E_{\lambda_1\sim\lambda_2}(\lambda,T)=\int_{\lambda_1}^{\lambda_2}\varepsilon(\lambda,T)E_{b\lambda}(\lambda,T)d\lambda\cong\sum\varepsilon(\lambda,T)E_{b\lambda}(\lambda,T)\Delta\lambda \tag{5}$$

Considering an aircraft coated with a full spectrum low-emissivity material (ε=0.2) at a cruising speed of Mach 2, the surface temperature is supposed to be 500 K, and the surface temperature increases with flight speed. Herein, from room temperature to 600K, the spectral

emissivity is independent of temperature, the $\varepsilon(\lambda,T) \approx \varepsilon(\lambda)$ is assumed.[8] Thus, the emissive power can only be correlated with temperature through the spectral irradiance of blackbody. Since the aim of the IR camouflage is to minimize the difference of thermal radiation between the object and the background, the method of determining the energy ratio between undetected bands and detected bands is reasonable.

The emissive power ratio from λ1 to λ2 between the designed surface and the reference surface was determined as follows:

$$\emptyset_{\lambda_1 \sim \lambda_2} = {}^{E_{\lambda_1 \sim \lambda_2, designed\ surface}}\Big/ E_{\lambda_1 \sim \lambda_2, reference\ surface} \tag{6}$$

In the undetected bands, the emissive power is the sum of 2.5~3 μm and 5~8 μm. Owing to IR detectors usually work in a single detected band (3~5 μm or 8~14 μm), the single-band CP (SCP) can be described as follows:

$$SCP = \emptyset_{undetected\ band}/\emptyset_{detected\ band} \tag{7}$$

Considering the dual detected band (λ1~λ2, λ3~λ4) simultaneously, the total CP (TCP) of designed ISE can be evaluated as follows:

$$TCP = CP(\lambda_1 \sim \lambda_2) \cdot CP(\lambda_3 \sim \lambda_4) \tag{8}$$

Note S7. The emissivity spectra of glass and reference

The glass (a soda-lime glass without deposited the proposed composite film) exhibits high emissivity in 2.5~14 μm band, and a nickel-based alloy film was employed as the reference sample (average emissivity in 2.5~14 μm is about 0.28), their emissivity spectra are shown in **Figure S7**. The thermal images can be captured by IR cameras with the working bands of 3~5 μm and 8~14 μm.

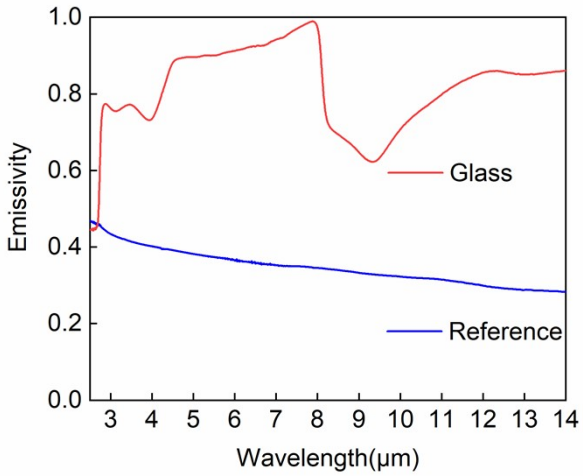

Figure S7. The emissivity spectra of glass and reference.

Note S8. Visual camouflage

We simulated the atmospheric transmission in visible band (400~780 nm) using MODTRAN (applying the midlatitude summer atmospheric model and rural aerosol model), as shown in **Figure S8a**. The spectrum does not have wavelength selective property. In visible band, the prepared single ITO film and single ZnS film both have high transmittance. In this study, desirable visible transmittance can be obtained by the composite multilayer of ITO and ZnS. Take sample #1 and #2 for example, the average transmittances are 67.5% and 82.4%, respectively. Thus, visible light is transmitted through the sample, providing transparency throughout the entire visible band.

For sample #2 of ITO/ZnS/ITO three-layer film structure, the top ITO and bottom ITO can reduce the reflectance, this may be the reason why the transmittance of sample #2 was better than that of single ZnS film in some regions. For sample #1 of ITO/ZnS/ITO/ZnS four-layer film structure, the transmittance of the composite film would be obviously decreased due to the additional ZnS film based on sample #2. The measured spectral transmittance curves of sample #1 and #2 are not smooth as those of single film, which can be explained by the theory of thin

film interference.[9] Owing to the half-wave loss, multiple resonances occur in the transmittance spectrum.

Figure S8b shows the schematic diagram of visible camouflage. The optically transparent infrared selective emitter with visible camouflage coating underneath is helpful to prevent visible detection of ground objects. As shown from **Figures S8c** to **S8e** . For various applied background, such as islands, jungles, deserts. Camouflage varies greatly for different applications. We covered ISE on different optical camouflage and observed its camouflage performance by optical camera. Compared with original optical camouflage, the ISE can preserve the camouflage performance of optical camouflages.

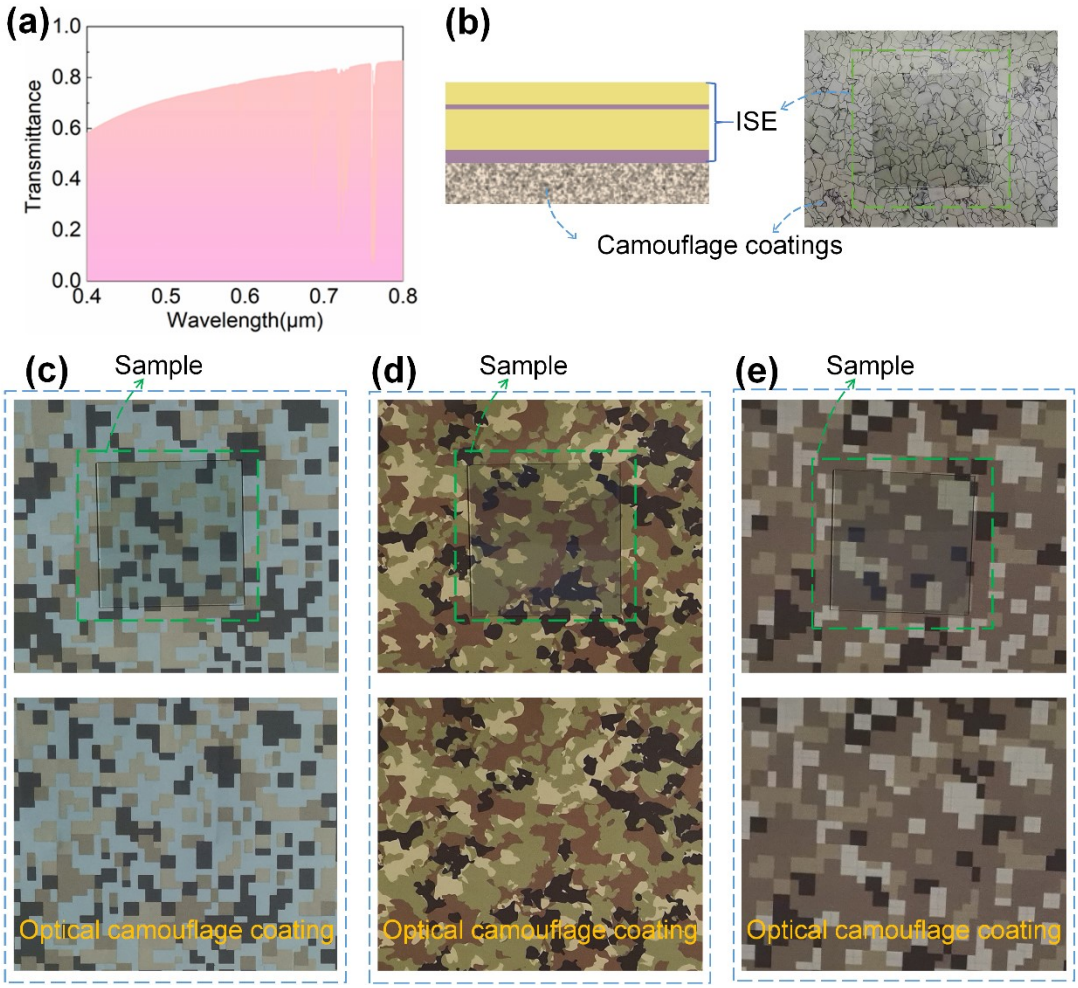

Figure S8. (a) The atmospheric transmission in visible band. (b) The schematic diagram of visual camouflage. (c), (d) and (e) demonstrate the camouflage peerformance in different backgrounds.

Note S9. Measuring method for spectral emissivity

At ambient temperature, the IR reflectance spectra were measured by Fourier transform infrared spectrometer (FTIR, Nicolet iS50, Thermo Fisher Scientific, spectral range: 2.5~25 μm) and the ultimate variable angle specular reflectance accessory (VeeMAX III, PIKE Technology). From monolayer to multilayer, the sample is positioned face down at the test site during measurement. In the ultimate variable angle specular reflectance accessory, the beams are reflected by three pairs of planar mirrors, a pair of curved mirrors and variable mirrors, converged on the test surface of the sample, as shown in **Figure S9**. Then the signal was reflected by the specular surface, which could be received by the receiver finally. At last, the time domain signal was processed by FFT method to generate a frequency domain reflectance spectrum. From monolayer to multilayer or relatively thick film, the sample is positioned face down at the test site during measurement. Experiments of monolayer and multilayer can be optimized by varying the angle of beam incidence. The emissivity in the range of 2.5~14 μm can be calculated by following equations:

$$\varepsilon_{2.5\sim14\mu m} = \frac{\int_{2.5\mu m}^{14\mu m} (1-\tau(\lambda)) M_{bb}(\lambda,T) d\lambda}{\int_{2.5\mu m}^{14\mu m} M_{bb}(\lambda,T) d\lambda} \quad (9)$$

The $M_{bb}(\lambda,T)$ stands for the blackbody emissive power at specified wavelength and temperature.

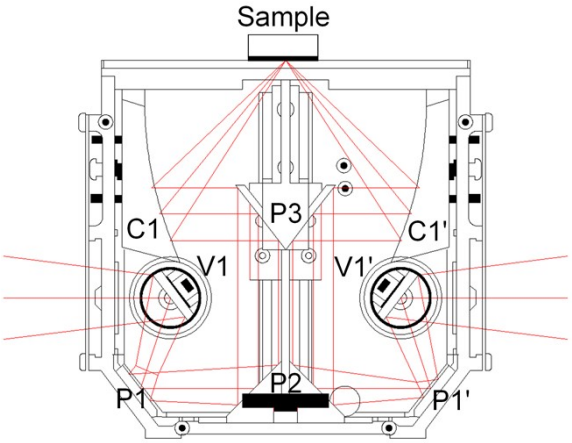

Figure S9. The proprietary beam path of ultimate variable angle specular reflectance accessory.

For measurements of the emissivity spectra at elevated temperatures, a cavity blackbody (ISDC-564/301) was introduced. When the sample is heated to a specified temperature by the heating device, the energy that the sample radiates outward is converted to the FTIR and eventually enter the IR detector. The emissive power of the blackbody $^{M_{bb}(\lambda,T)}$ and that of the sample $^{M_s(\lambda,T)}$ can be measured by optical device at the same temperature, the emissivity can be expressed as:

$$\varepsilon = \frac{M_{sample}(\lambda,T)}{M_{bb}(\lambda,T)} \tag{10}$$

Note S10. Working temperature range of ISE

Owing to the fact that the flight speed is too fast, the surface will have a drastic friction with the air, which will lead to the rapid increase of surface temperature. For example, when SR-71 flying with a speed of Mach 3, the surface temperature can reach more than 300 ℃. When the flight speed exceeds Mach 3, the hearing and thermal disabilities occur on the aircraft (aircraft with an alloyed surface). As a result, to assure the safety of pilot, the maximum speed of fighter was maintained around Mach 2 to 3 in most situations.

In this work, we choose 600 K as the standard to evaluate the infrared camouflage

performance. The state about 500 K is just an example of supersonic vehicle, which provides a practical environment to help us to understand the temperature about serving aircraft. To verify whether the ISE can serve steadily at the temperature of 600 K, we tested the thermal stability of ISE up to 700 K. Stable emissivity spectra can be observed from 300 K to 700 K, which verify the stability of the ISE. This redundant temperature design can significantly guarantee its thermal stability from room temperature to 600 K.

Note S11. The stability of ZnS and the superiority of the composite structure

We discussed the stability of solid-ZnS in forms of powder, ceramic and film. ZnS powder possesses well stability in dry environment. Its α phase (hexagonal phase) has a melting point of 1700℃ and 1020℃ transformed into β phase (cubic crystal phase). ZnS powder can be oxidized to ZnSO4 in humid environment, but the moisture evaporated obviously while cruising, which is beneficial for the practical application of ZnS. ZnS ceramic, possesses a melting point of 1830℃, is the preferred material for fairing of long wave infrared precision guided missile. ZnS lenses and ZnS film are widely used in infrared detector window, infrared imaging system, and infrared lidar sealing cover, etc. These applications demonstrate that ZnS can exist stable in air. In this paper, the composite ITO/ZnS multilayers were heated repeatedly in practical environment to measure spectral thermal emissivity and obtained stable results. The stability of the composite sample can be verified by experimental test.

ZnS film is transparent in the wavelength from 0.35 to 14 μm, which is suitable for designing infrared-visible compatible materials. Herein, it was employed to design infrared selective emitter with high visible transmittance for the first time.

We demonstrated the reliability of ZnS and superiority of this composite structure by

comparing with relevant literature and data. ZnS can be used for fabricating metamaterial-based ISEs. For example, Lee et. al. proposed a metamaterials-based ISE, which evaluated total camouflage performance of Au/ZnS/Au metamaterials from 300K to 600K.[6,10] Besides, unlike metamaterial-based ISEs, the entire preparation process of the proposed composite structure avoids planar fabrication of sub-wavelength unit patterns, thus eliminating photolithography and etching. The sample can exhibit enhanced structural stability while retaining excellent selective emission.

ZnS are widely used for designing photonics crystal based ISEs and multilayer film based ISEs. As shown in **Table 2** and **Table 3**, layers are numerous and opaque for the photonic crystal based ISE[11-13] and multilayer film based ISE[14-16]. Our work not only simplifies the structure of ISE, but also is compatible with visible transmittance. Moreover, the camouflage performance is effective from room temperature to 600 K. An additional test at 700 K for 1 hour proved that the sample can possesses stable thermal emissivity in practical using.

In summary, this work exhibits desirable selective emissivity and visible transmittance for infrared-visible camouflage. The four-layer composite film without in-plane structure is suitable for scalable manufacturing and long-time serving.

Table 1 photonic crystal based ISE:

reference	materials	functional band/μm	layers	thickness/μm
[11]	Ge/ZnS	3~5	10	3.525
[12]	Ge/ZnS	3~5, 8~14	20	12.09
[13]	Ge/ZnS	3~5, 8~14	48	29.898

Table 2 multilayer film based ISE:

reference	materials	functional band/μm	layers	thickness/μm
[14]	Ge/ZnS	8~14	13	11.9
[15]	Ge/ZnS	3~5, 8~14	9	8.975

[16]	Ge/ZnS	3~5, 8~14	13	6.732

Table 3 this work:

	materials	functional band/μm	layers	thickness/μm
This work	ITO/ZnS	0.4~0.8, 3~5, 8~14	4	1.95

In this frame, more infrared transmissive materials can be selected as dielectrics to design ISEs with higher temperature using, such as HfO_2 and AlON, etc.[17-19] This work is neither a simple alternating composite of ITO and ZnS films, nor the method for designing the ISE based on photonic crystals or conventional multilayer films. In this design, desirable performance with the simplest constructs can be achieved by combining Drude model and the size effect of ITO film. The core idea can be summarized as simple in geometry, functional in using, but complex in mechanism.

Table 4 High temperature Infrared transmissive materials

materials	energy gap/eV	short-wave cut-off limit/μm	pass band/μm	melting point/℃
ZnS	3.5	0.35	0.35~14	1830
Al_2O_3	9	0.14	0.14~6	2045
AlON	6.5	0.19	0.2~5.5	2140
HfO_2	5.4	0.23	0.23~7	2800

Reference

1 P. Chelvanathan, Y. Yusoff, F. Haque, M. Akhtaruzzaman, M. Alam, Z. Alothman, M. J. Rashid, K. Sopian and N. Amin, *Appl. Surf. Sci.*, 2015, **334**, 138–144.

2 Y. Subbaiah, P. Prathap and K. Reddy, *Appl. Surf. Sci.*, 2006, **253**, 2409–2415.

3 M. Zhang, X. Ma, J. Yin, Y. Zhang, L. Zhang, J. Wen, L. Dai, R. Kuang, H. Chen, X. Weng,

X. Zhao, D. Liang, J. Xie and L. Deng, *Appl. Surf. Sci.*, 2020, **532**, 147280.

4 J. K. Pradhan, S. A. Ramakrishna, B. Rajeswaran, A. M. Umarji, V. Achanta, A. Agarwal and A. Ghosh, *Opt. Express*, 2017, **25 8**, 9116–9121.

5 H. Tian, H. Liu and H. Cheng, *Compos. Sci. Technol.*, 2014, **90**, 202–208.

6 N. Lee, T. Kim, J. S. Lim, I. Chang and H. Cho, *ACS Appl. Mater. Interfaces*, 2019, **11 23**, 21250–21257.

7 Y. Cengel and A. J. Ghajar, 2013.

8 X. Liu, T. Tyler, T. Starr, A. Starr, N. Jokerst and W. J. Padilla, *Phys. Rev. Lett.*, 2011, **107 4**, 45901.

9 J. Zhang, R. Liu, D. Zhao, H. Wang, Y. Zhang, C. Wang and J. Shi, *Opt. Mater. Express*, 2019, **9**, 195–202.

10 T. Kim, J. Y. Bae, N. Lee and H. Cho, *Adv. Funct. Mater.*, 2019, **29**, 1807319.

11 W. Zhang, G. Xu, F. Shi, H. Ma and L. Li, *Photonics Nanostructures Fundam. Appl.*, 2015, **14**, 46–51.

12 W. Zhang, G. Xu, J. Zhang, H. Wang and H. Hou, *Opt. Mater.*, 2014, **37**, 343–346.

13 Z. Wang, Y. Cheng, Y. Nie, X. Wang and R. Gong, *J. Appl. Phys.*, 2014, **116**, 54905.

14 D. Qi, F. Chen, X. Wang, H. Luo, Y. Cheng, X. Niu and R. Gong, *Opt. Lett.*, 2018, **43 21**, 5323–5326.

15 H. Zhu, Q. Li, C. Zheng, Y. Hong, Z. Xu, H. Wang, W. Shen, S. Kaur, P. Ghosh and M. Qiu, *Light. Sci. Appl.* 2020, **9**.

16 H. Zhu, Q. Li, C. Tao, Y.-M. Hong, Z. Xu, W. Shen, S. Kaur, P. Ghosh and M. Qiu, *Nat. Commun.2021, **3**.*

17 P. Dyachenko, S. Molesky, A. Petrov, M. Stoermer, T. Krekeler, S. Lang, M. Ritter, Z.

Jacob and M. Eich, *Nat. Commun.* 2016, 7.

18 Y. Shan, X. Wei, X. Sun, J. Xu, Q. Qin and E. Olevsky, *J. Mater. Res.*, 2017, **32**, 3279–3285.

19 P. Zhang, Z. Ye, C. H. Sun, Y. Chen, T. Zhang, X. Chen, C. Lin, R. Ding and L. He, *J. Electron. Mater.*, 2016, **45**, 4716–4720.